https://doi.org/10.22226/2410-3535-2022-4-287-291

Microstructure of the deposited NiCrBSiC coating after laser polishing

L. E. Afanasieva[†,1], I. S. Pavlov[2]

[†]ludmila.a@mail.ru

[1]Tver State Technical University, Tver, 170026, Russia
[2]FSRC "Crystallography and Photonics" RAS, Moscow, 119333, Russia

The structure of the surface layers of NiCrBSiC coatings obtained by powder laser cladding and subsequent laser polishing with a multichannel CO_2 laser has been studied. XRD and TEM/STEM showed that the coatings are a γ-Ni matrix with Ni_3B, Cr_3C_2 and Ni_3Si precipitates. It was shown that the matrix of the coating after laser cladding has a high density of dislocations, which form networks. XRD evidences a decrease in the number of the precipitates after laser polishing and TEM/STEM demonstrated a decrease in the density of dislocations and the appearance of nanostructured γ-Ni layers in the form of flat elongated plates. The width of nano-grains is ≈20 nm near the interface and increases with distance from it. Microhardness measurements showed an increase from 4.4 to 5 GPa after laser polishing.

Keywords: coating, NiCrBSiC alloy, laser cladding, laser polishing, TEM, XRD.

1. Introduction

The NiCrBSiC alloy is a well-known wear and corrosion resistant self-fluxing material, which is used as a coating with excellent mechanical properties [1–3]. This is a Ni-based alloy with precipitates of borides, carbides and silicon-containing phases of various sizes and shapes [4]. Such coatings are widely used to restore worn parts and improve the performance characteristics of new parts, which operate under conditions of high contact loads, aggressive environments and elevated temperatures. For example, it is useful in the aerospace, oil and gas, transportation, energy and mining industries [5–7]. There are a lot of methods for cladding of this coating: electric arc, gas, laser, cladding by high frequency currents as well as hybrid technologies are applied [7–13]. In comparison with others, laser cladding has several advantages [9–11]. It allows forming cladding layers with a low mixing ratio because of slight penetration of the substrate and this layer has satisfactory adhesion with the substrate. Moreover, laser cladding contributes to the processing locality, uniformity of the applied coating thickness, small heat affected zone and small residual deformations of cladded parts. It should be also noticed that laser cladding conditions influence the microstructure of alloys that changing their properties [2].

In practice, cladding of coatings with a specified surface roughness is an important task especially for precision parts and assemblies. Coatings after laser cladding have significant waviness and roughness and require grinding with abrasive wheels. It is known that dangerous tensile stresses that reduce fatigue resistance appear in surface layers after traditional mechanical grinding. The formation of microcracks and burns is also possible [9]. Automation of mechanical grinding and polishing of parts that have complicated shapes is a serious challenge and manual labor decreases efficiency and increases cost.

The noted disadvantages can be partially corrected by using laser polishing [14–20]. The effectiveness of laser polishing in metal finishing has been successfully demonstrated for tool and stainless steels, nickel and titanium alloys, and other materials. A thin layer of the material melts under laser radiation during polishing and smoothing of surface topography as a result. The novelty and complexity of the method stimulated many experimental studies aimed to determine the laser exposure modes, which lead to proper quality of the surface [8,15–18]. In our previous work, we demonstrated that the maximum wave height W_{max} of the NiCrBSiC alloys decreases in 3 times (from 60 to 18 μm) after laser polishing [11]. Optimization of technological parameters can reduce the final roughness of the laser-polished surface to nanometers. For example, some classes of metal alloys can have an average roughness of the surface around 5 nm [16].

However, an incomplete understanding of the fundamental mechanisms underlying this technology prevents the wide industrial implementation of laser polishing. A nonequilibrium multicomponent thermodynamic process leads to the formation of complex microstructures. This process is poorly studied, however, microstructures have a crucial influence on such performance properties as wear resistance and others. The purpose of this study is the electron microscopy and X-ray diffraction (XRD) analysis of the microstructure of the cladded NiCrBSiC coating after laser polishing.

2. Experimental procedures

Powder cladding and subsequent melting of the surface layers of the NiCrBSiC coating were conducted by a multichannel (40 beams) CO_2-laser using a facility of the model ALTKU-3 at the Laser Technology Center in Vladimir. The radiation power during cladding was 2.3 kW and the spot diameter was 6 mm. The speed of the laser beam moving along the deposited surface was 3 mm/s. The clad material was a nickel-base self-fluxing granulated powder of grade PG-19N-01 with the following chemical composition (in wt.%): 0.3 – 0.6 C, 3.9 –14 Cr, 1.7 – 2.5 B, 1.2 – 3.2 Si, 3.2 – 5.0 Fe, 0.8 –1.3 Al, the remainder Ni (TU 48-190383-91). The substrate material was structural steel 30 (GOST 1050-88). A two-step method was applied for cladding. The filler material was deposited preliminarily onto the surface of the substrate with a special stencil, levelled over the thickness, and melted by continuous laser radiation with 30% overlapping of the beads. Then, the second layer was deposited and melted. After cladding, laser polishing was carried out by repetitively pulsed radiation with a power of 2.5 kW. The spot diameter and the speed of the laser beam were 6 mm and 15 mm/s correspondingly.

The study of morphology and analysis of the elemental composition was conducted on a scanning electron microscope (SEM)/focus ion beam (FIB) Scios (ThermoFisher Scientific, USA). Specimens for transmission and scanning transmission electron microscopy (TEM and STEM, correspondingly) were prepared according to the standard lift-out FIB technique in a FIB/SEM dual-beam Scios (Thermo Fisher Scientific, USA) at an accelerating voltage of Ga^+ ions of 30 kV at the first steps and 2 kV at the final steps of ion etching. Microstructural analyses were performed in an OSIRIS TEM/STEM (Thermo Fisher Scientific, USA) equipped with a high angle annular dark-field (HAADF) electron detector (Fischione, USA) and a Bruker super X energy-dispersive X-ray (EDX) microanalysis system (Bruker, USA) at an accelerating voltage of 200 kV. Image processing was performed using a Digital Micrograph (Gatan, USA) and TIA (ThermoFisher Scientific, USA) software.

The XRD measurements were carried out on a Bruker D8 Advance diffractometer (Bruker, USA) using $Co_{K\alpha}$ radiation (40 kV, 15 mA, Ni-Kβ filter) in the angular range of $2\theta = 3 – 120°$ with a scanning step of 0.02° and a speed of 0.5°/min. The size of the beam incident on the sample was set by horizontal and vertical slits, 10 mm and 1.25°, respectively. Phase identification was performed using the PDXL program (Rigaku Corporation, Japan) using the ICDD PDF-2 database (2017).

The microhardness was measured by the method of the reconstructed indent using a PMT-3 device according to the GOST P 8.748-2011 (ESO 14577-1:2002) standard at a force of 0.98 N.

3. Results

SEM image of the cross section of the NiCrBSiC coating on the steel substrate is presented in Fig. 1. The thickness of the coating is 2 mm and it has the characteristic for laser cladding homogeneity [7, 9 –11].

XRD spectrum of the coating after laser cladding (Fig. 2 a) indicates the presence of γ-Ni with the space group $Fm\bar{3}m$ [21] and Ni_3B — Pnma [22]. The low peak around 30° (3.51 Å) can be associated with Ni_3Si ($Pm\bar{3}m$) [23]. The peak around 52° (2.04 Å) has a shoulder. This shoulder can indicate the presence an additional phase, which has a close peak. We suppose that this phase is Cr_3C_2 with the space group Cmcm [24]. The spectrum after laser polishing is presented in Fig. 2 b. We can identify almost all the previous peaks. However, intensity all of them except for Ni are less and for this reason, we do not see the shoulder that was attributed to Cr_3C_2.

The HAADF image of the cross section of the coating after laser cladding is presented in Fig. 3 a. In such images, the contrast depends on the atomic numbers of contained elements — a darker area has more light elements. Pt layers were applied on the surface by electron (thin gray layer)

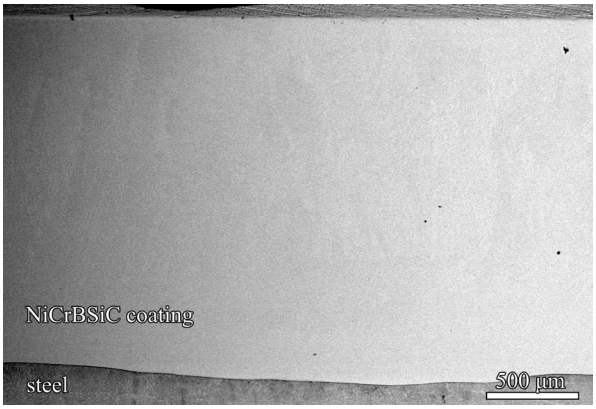

Fig. 1. SEM image of the cross section of the NiCrBSiC coating on the steel substrate.

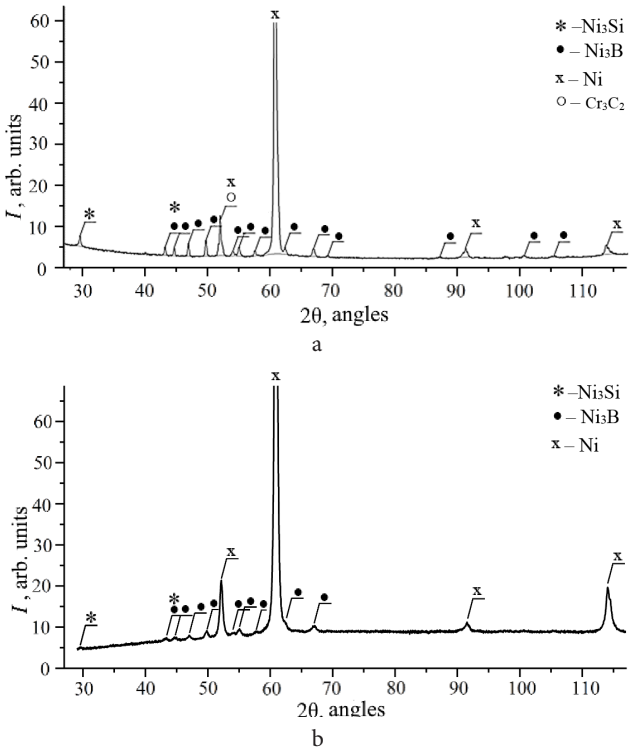

Fig. 2. XRD spectrum of the NiCrBSiC coating after laser cladding (a) and after laser polishing (b).

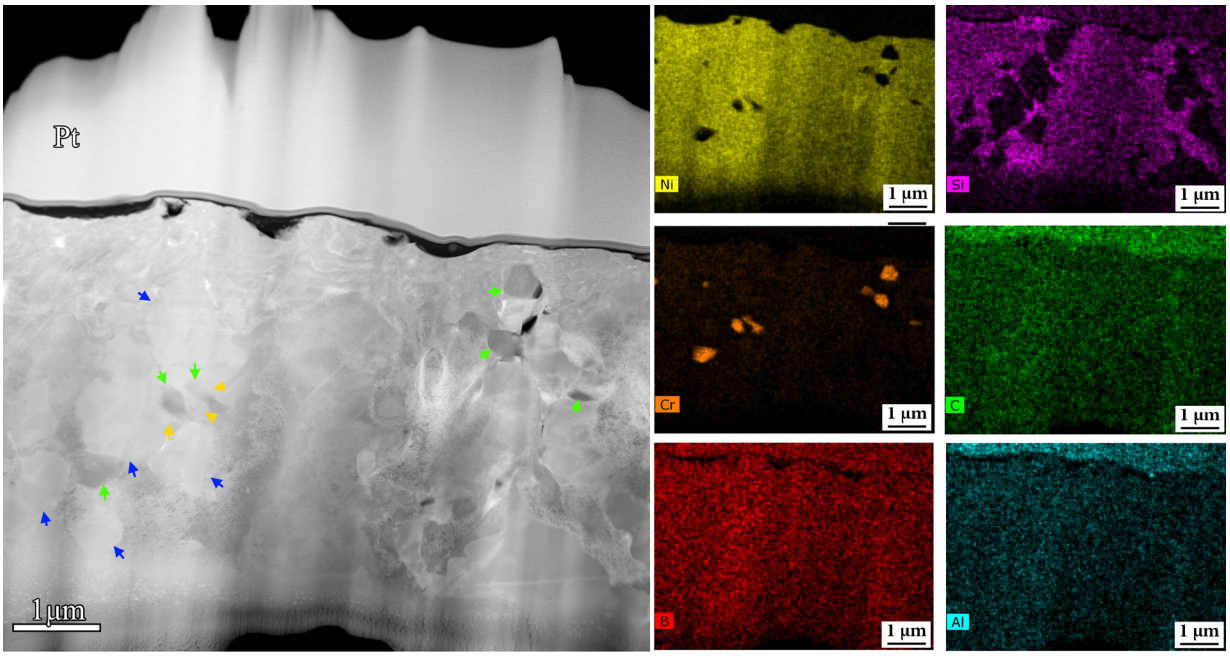

a b

Fig. 3. (Color online) HAADF image of a cross section of the NiCrBSiC coating after laser cladding. Dark blue arrows mark precipitates of Ni_3B, green arrows — Cr_3C_2, yellow arrows — Ni_3Si (a); EDX maps of distribution of elements (b).

and ion (thick bright layer) beams to protect it during FIB preparation. The HAADF image and EDX maps (Fig. 3) allow one to locate phases, which were observed by XRD. Selected area electron diffraction patterns (SAEDP) of areas with different compositions are shown in Fig. 4. The top-left SAEDP is in agreement with γ-Ni, the [110] zone axis of which is parallel to the electron beam. The top-right SAEDP corresponds to Cr_3C_2 that is oriented parallel to [100]. Bottom left — Ni_3Si parallel to [110] and bottom right — Ni_3B parallel to $[01\bar{1}]$. These phases are precipitates in the γ-Ni matrix. Some precipitates of Ni_3B are marked with dark blue arrows in Fig. 3, Cr_3C_2 are marked with green arrows and Ni_3Si — yellow arrows. It can be noticed that the main part of Si is distributed around boundaries between different phases and Ni_3Si formed between Ni_3B and Cr_3C_2. The concentration of Ni_3B precipitates measured from HAADF images is 0.2 μm^{-2} and their average size is 0.9 μm. Precipitates of Cr_3C_2 have a concentration and an average size of 0.3 μm^{-2} and 0.3 μm correspondingly. Ni_3Si — 0.2 μm^{-2} and 0.2 μm.

The HAADF image after laser polishing is presented in Fig. 5. The matrix consists of the same precipitates as before polishing (Figs. 2, 3, 4), which are marked by the same arrows. The concentration of Ni_3B is 0.3 μm^{-2} and the average size is 0.6 μm. The measured concentration and average size of Cr_3C_2 precipitates is 0.1 μm^{-2} and 0.4 μm. Ni_3Si precipitates have a concentration of 0.2 μm^{-2} and an average size of 0.15 μm. Nanostructured grains of γ-Ni appeared near the interface after polishing (Fig. 5 b). They are flat and retracted and have a width of about 20 nm near the interface, increasing with distance from it. The angle of misorientation of these grains with the interface is ≈20°.

A rhombic dislocation network is visible on a bright-field (BF) STEM image acquired around 3 μm from the surface of the laser-cladded sample (Fig. 6 a). Besides the network, separated dislocations are also visible. A large number of

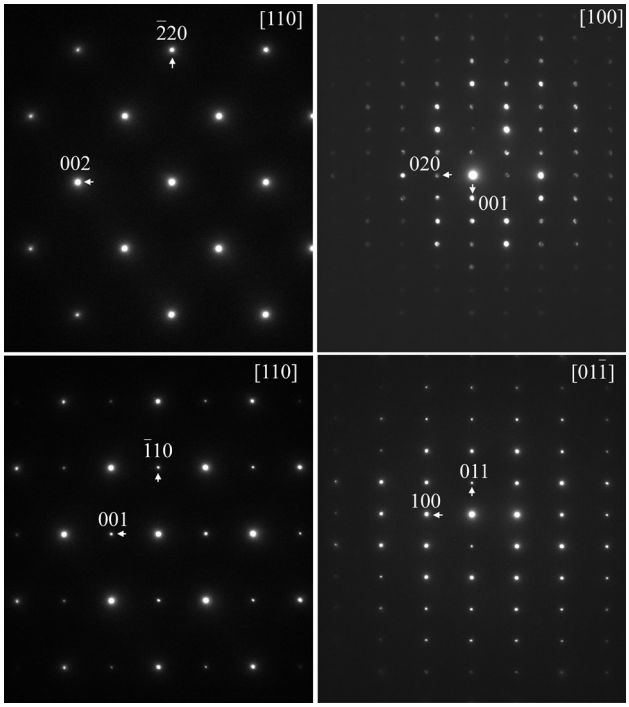

Fig. 4. SAEDPs of the γ-Ni matrix (top left) and precipitates Cr_3C_2 (top right), Ni_3Si (bottom left) and Ni_3B (bottom right). Their orientations relative to the electron beam are parallel to [110], [100], [110] and $[01\bar{1}]$ zone axis, correspondingly.

different defects complicates quantification of the density of dislocations. However, it must be noticed that this density is very high. Rhombic networks miss after laser polishing. Nevertheless, nodes, loops and separated dislocations are available (Fig. 6 b), but their density seems to be lower.

Microhardness measured after laser cladding and after laser polishing is 4.4 and 5 GPa correspondingly.

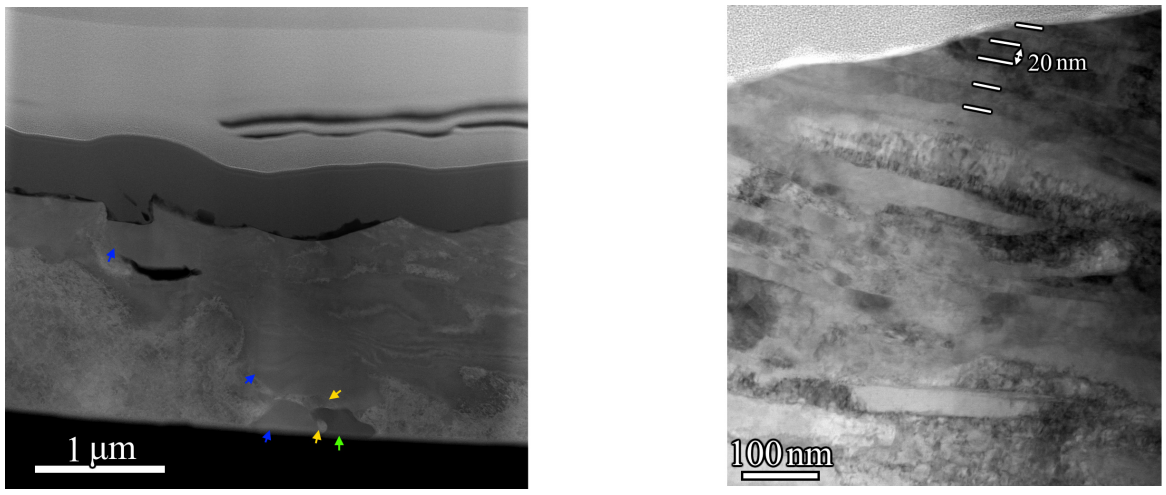

a b

Fig. 5. (Color online) HAADF image of the cross section of the NiCrBSiC coating after laser polishing. Dark blue arrows mark precipitates of Ni_3B, green arrows — Cr_3C_2, yellow arrows — Ni_3Si (a); bright-field high resolution STEM image of the interface (b).

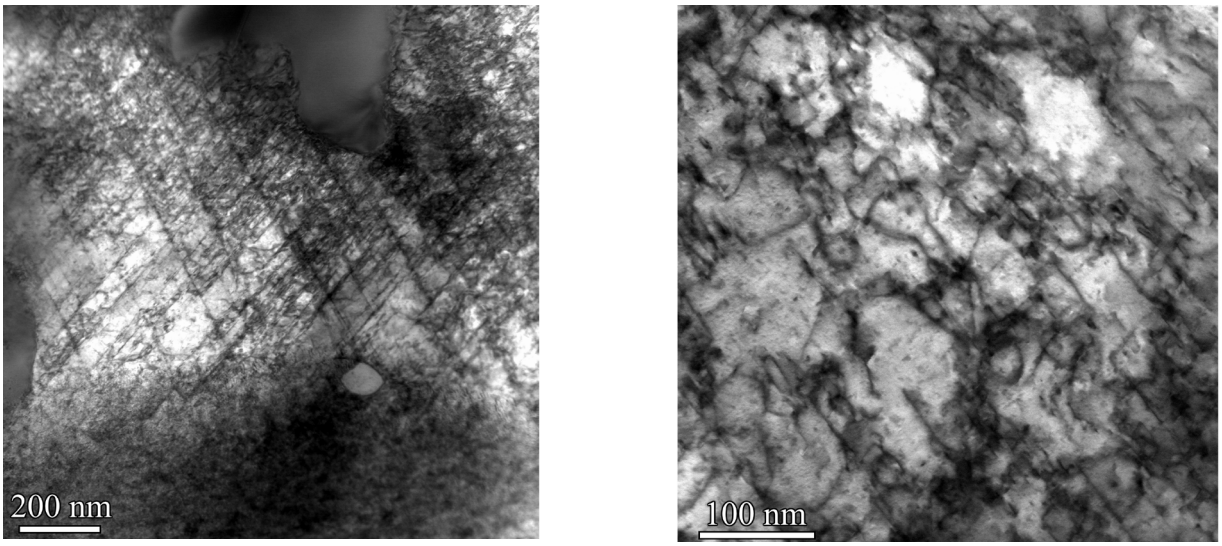

a b

Fig. 6. STEM BF image of dislocations near the surface of the laser-cladded material before (a) and after laser polishing (b).

4. Discussion

Despite the fact that the processes of laser cladding and laser polishing are very close, they have several differences. With laser polishing, the radiation penetrates the material to a less depth than with laser cladding. Due to this, laser polishing melts thinner areas and therefore heat rejection is more efficient. Besides, repetitively pulsed laser processing can be a source of impact interactions. These differences lead to a change in the microstructure and properties of the coating.

TEM and XRD studies (Figs. 2, 3, 4) did not show changes of the phase composition of the coating after laser polishing. The decrease in the intensity of peaks of the XRD spectrum (Fig. 2) from Ni_3B, Ni_3Si and Cr_3C_2 probably relates to a decrease in the concentration of these phase. TEM studies have not confirmed significant changes in their concentrations and average sizes (Fig. 3, 5), however we must take into account that this method is very local. Such a decrease in the concentrations of the precipitates could be realized by increasing the solubility limit of γ-Ni, which can be due increasing of the rate of the heat rejection.

According to literature [25, 26], grain boundaries and boundaries of precipitates are dislocation nucleation sites as well as catching them. For this reason, we can see a significant number of dislocations in the coating after laser cladding. Increasing the amount of dislocations leads to the formation of networks because such distribution of them requires the lowest energy. Generally, a subsequent increase in their number contributes to the separation of grains and the formation of several misorientated grains with low angle boundaries. Reducing the number of precipitates contributes to a decrease in the density of dislocations that was demonstrated in Fig. 6. Impact interactions during laser polishing, in turn, should increase the number of dislocations and we propose that this effect is leveled out by dividing γ-Ni grains to nano-grains, which we see in Fig. 5 b. The appearance of nano-grains can be responsible for the increase in microhardness.

One of the most important features of NiCrBSiC coatings is wear resistance and it could be estimated by the Eq. (1) [27]:

$$\frac{dx}{dV} = \frac{\sigma_0}{kF_N} x, \qquad (1)$$

where V is volumetric wear; F_N — normal force; σ_0 and k are hardness and wear factor (depends on the geometry of the abrasive surface) correspondingly. According to Eq. (1), an increase in microhardness must lead to improvement of wear resistant. For this reason, laser polishing contributes to the formation of surfaces with advanced tribological properties. Replacing of traditional mechanical grinding with laser polishing in manufactures would reduce the coast of products and increase the productivity and automation of the process.

5. Conclusion

NiCrBSiC coatings were obtained on steel 30 by powder laser cladding and subsequent laser polishing with a multichannel CO_2-laser. XRD and TEM/STEM demonstrated that such coatings are a γ-Ni matrix with Ni_3B, Cr_3C_2 and Ni_3Si precipitates. After laser polishing, XRD studies showed a decrease in the density of precipitates and TEM/STEM showed a decrease in the number of dislocations and the appearance of nano-grains of γ-Ni near the interface. At the same time, microhardness raised after laser polishing.

Acknowledgements. We are grateful to A. A. Nikitin for the consultation during making the research. This work was supported by the Ministry of Science and Higher Education of Russian Federation within the State assignment Federal Scientific Research Centre "Crystallography and Photonics" of Russian Academy of Sciences and was performed using the equipment of the Shared Research Centre of the FSRC "Crystallography and Photonics" of RAS.

References

1. X. Yan, S. Gao, C. Chang, J. Huang, K. Khanlari, D. Dong, W. Ma, N. Fenineche, H. Liao, M. Liu. Journal of Materials Processing Technology. 288, 116878 (2021). Crossref
2. O. G. Devojno, E. Feldshtein, M. A. Kardapolava, N. I. Lutsko. Optics and Lasers in Engineering. 106, 32 (2018). Crossref
3. E. J. Chun, C. Park, H. Nishikawa, M. S. Kim. Applied Surface Science. 442, 726 (2018). Crossref
4. I. Hemmati, J. C. Rao, V. Ocelík, J. T. M. De Hosson. Microscopy and Microanalysis. 19 (1), 120 (2013). Crossref
5. X. Yan, C. Chang, Z. Deng, B. Lu, Q. Chu, X. Chen, W. Ma, H. Liao, M. Liu. Tribology International. 157, 106873 (2021). Crossref
6. L. E. Afanasieva, G. V. Ratkevich. Letters on Materials, 8 (3), 268 (2018). (in Russian) Crossref
7. L. E. Afanas'eva, G. V. Ratkevich, M. V. Novoselova. Metal Science and Heat Treatment. 61, 581 (2020). Crossref
8. R. Gonzalez, M. Cadenas, R. Fernandez, J. L. Cortizo, E. Rodríguez. Wear. 262 (3 – 4), 301 (2007). Crossref
9. N. N. Soboleva, A. V. Makarov, I. Yu. Malygina. Metal processing (technology, equipment, tools). 4 (61), 79 (2013). (in Russian)
10. N. Serres, F. Hlawka, S. Costil, C. Langlade, F. Machi. Journal of thermal spray technology. 20, 336 (2011). Crossref
11. V. I. Yugov, L. E. Afanasieva, M. V. Novoselova. Hardening technologies and coatings. 11 (143), 19 (2016). (in Russian)
12. Z. Bergant, J. Grum. Journal of thermal spray technology. 18, 380 (2009). Crossref
13. A. A. Burtsev, O. Ya. Butkovskiy. Physical and chemical aspects of the study of clusters, nanostructures and nanomaterials. 11, 107 (2019). (in Russian) Crossref
14. T. Ermergen, F. Taylan. Arabian Journal for Science and Engineering. 46, 7125 (2021). Crossref
15. A. Gisario, M. Barletta, F. Veniali. The International Journal of Advanced Manufacturing Technology. 120, 1 (2022). Crossref
16. E. V. Bordatchev, A. M. K. Hafiz, O. R. Tutunea-Fatan. The International Journal of Advanced Manufacturing Technology. 73, 35 (2014). Crossref
17. E. Ukar, A. Lamikiz, L. L. de Lacalle, D. Del Pozo, J. L. Arana. International Journal of machine tools and manufacture. 50 (1), 115 (2010). Crossref
18. L. Chen, B. Richter, X. Zhang, K. B. Bertsch, D. J. Thoma, F. E. Pfefferkorn. Materials Science and Engineering: A. 802, 140579 (2021). Crossref
19. Y. Liu, W. Ouyang, H. Wu, Z. Xu, L. Sheng, Q. Zou, J. Jiao. Journal of Materials Processing Technology. 300, 117428 (2022). Crossref
20. B. Zhang, H. Yang, H. Liu, J. Hao, X. Liu. Applied Surface Science. 573, 151557 (2022). Crossref
21. A. W. Hull. Physical Review. 10, 661 (1917). Crossref
22. G. F. Kayser, F. X. Kayser. Journal of Alloys and Compounds. 233, 74 (1996). Crossref
23. N. F. Lashko. Doklady Akademii Nauk SSSR. 81, 606 (1951). (in Russian)
24. E. Bouzy, E. Buer-Grosse, G. Le Caër. Philosophical Magazine Part B. 68 (5), 619 (1993). Crossref
25. I. I. Novikov. Defects in the crystal structure of metals. Moscow, Metallurgiya (1975) 208 p. (in Russian)
26. J. Friedel. Dislocations: international series of monographs on solid state physics. V. 3. Elsevier (2013) 660 p.
27. V. L. Popov. Contact interaction mechanics and friction physics. From nanotribology to earthquake dynamics. Moscow, Fizmatlit (2013) 352 p. (in Russian)